PAPER 5

Multitemporal analysis of forest biomass using AIRSAR data

In: Proceedings of the 25th International Symposium, Remote Sensing and Global Environmental Change, Graz, Austria, 4–8 April, 1993. Pp. I-328–I-338.

MULTITEMPORAL ANALYSIS OF FOREST BIOMASS USING AIRSAR DATA*

Yrjö Rauste
Technical Research Centre of Finland
Instrument Laboratory
Espoo, Finland

ABSTRACT

Multitemporal AIRSAR data of the Freiburg test site of the MAESTRO-1 and MAC Europe campaigns were used for forest biomass mapping. Image data acquired in August 1989, June 1991, and July 1991 were geo-coded to the same grid structure. A geocoding residual error less than 2 pixels (less than 20 m) was achieved using a DEM. The HV-polarization of P-band was verified to be the optimal band-polarization combination in forest biomass mapping. A multitemporal regression model produced a higher correlation (0.82) between forest biomass and radar data than the highest single-date correlation (0.79). Clear-cut areas could be identified in multitemporal radar data in all three bands studied: C, L, and P.

1 INTRODUCTION

Accurate knowledge on the amount and spatial distribution of forest biomass is essential in environmental and climatological modelling. In large areas of the world, timber is also a valuable natural resource for paper and sawmill industries and an important source of energy.

Radar has been studied as a tool for forest inventory fairly widely (e.g. Sader 1987, Hussin et al. 1991, Christensen et al. 1990, Kasischke et al. 1991, and Le Toan et Beaudoin 1991). Radar, due to its cloud-penetrating capability, is very suitable for multitemporal analysis. Only few studies (e.g. Rignot et al. 1992) have concentrated on the use of multitemporal radar data in forest inventory applications.

The radar data used in this study have been acquired in two international research campaigns: MAESTRO-1 (1989-1992, organized jointly by the Joint Research Centre of EC and the European Space agency) and MAC Europe (1991, organized mainly by NASA).

The objective of this study is to assess the potential of multitemporal radar data in forest biomass mapping.

*Presented at the 25th International Symposium, Remote Sensing and Global Environmental Change, Graz, Austria, 4-8 April 1993

2 MATERIALS AND METHODS

2.1 Ground data

The forested study site (centre: 48°05'25" N, 8°22'01" E) is in Germany close to the town Villingen-Schwenningen. The main tree species are Norway spruce (*Picea abies*), fir (*Abies alba*), and Scotch pine (*Pinus sylvestris*). Deciduous trees are rare in the study site. The area is relatively flat although the elevation (750 m ... 970 m above mean sea level) is high.

The forest inventory ground data consist of two elements:

- a forest map in scale 1:10 000 showing the stands and
- forest inventory data sheets.

The forest inventory data sheets contain for every stand:

- the area of the stand,
- stem volume, and
- the distribution of the area among tree species.

The forest map and the forest inventory data sheets describe the situation in October 1981. The map was digitized and converted into a raster image. From the forest inventory data sheets, the items mentioned above were input into the computer system used. The forest stem volume data were used as a substitute for biomass data because no data on total biomass was available. The amount of total biomass can be assumed to be directly proportional to the stem volume.

The digital elevation model (DEM) used in geocoding of AIRSAR data was generated by the Universität Stuttgart/Institut für Navigation. Contours from the German topographic maps in scale 1:50 000 were used as input to the DEM generation.

2.2 AIRSAR Data

The SAR data were acquired by the AIRSAR system (Held et al. 1988) operated by NASA/JPL. SAR data from three days were studied:

1. 18 August 1989 (CCT id HR1105C, HR1105L, and HR1105P),
2. 15 June 1991 (CCT id CM3169), and
3. 16 July 1991 (CCT id CM3275).

The first scene was acquired in the MAESTRO-1 campaign (Churchill et Attema 1991) and the other two scenes in the MAC Europe campaign. The first scene is in single-look scattering matrix format, the other two scenes in 16-look compressed Stokes matrix format.

2.3 Preprocessing of AIRSAR Data

2.3.1 Calibration

The August-89 scene was calibrated (Rauste 1992b) using trihedral reflectors and the algorithms described by van Zyl (1990) and Zebker et Lou (1990).

The June-91 scene was phase calibrated using trihedral corner reflectors. For the P-band calibration, a 5-m high trihedral corner reflector was constructed of chicken-wire. Neither cross-talk removal, nor channel balance calibration was applied. In the June-91 scene, the average return power decreased with increasing range much stronger than in the August-89 or July-91 scenes. Because the reason for this steeper decrease was not known (possibly uncertainty in antenna pattern correction in the SAR processor) a very simple correction was applied. A linear regression line was determined for the June-91 and July-91 scenes. The June-91 scene was subsequently multiplied by a range-dependent constant in such a way that the slope of the regression line of the June-91 was forced to that of the July-91 scene.

The July-1991 scene was calibrated (phase calibration, cross-talk, and channel imbalance) by JPL.

2.3.2 Forming of the multitemporal image database

Quantitative analysis of multitemporal remote sensing data is facilitated considerably if the image data are resampled to the same, geo-referenced grid. The geo-coding of the AIRSAR data was done using polynomial rectification with a digital elevation model. The resampling was done on Stokes matrix data, separately for each element of the Stokes matrix. The August-89 scene, which originally was in single-look scattering matrix format, was first converted to Stokes matrix format and compressed using the algorithm described by Dubois et Norikane (1987).

In the polynomial rectification, the relationship between object space (geodetic) co-ordinates and the image co-ordinates (range and azimuth) is expressed in the form of polynomial functions whose coefficients are determined using ground control points (GCP). The relief displacement is treated separately as an elevation-dependent correction to the range co-ordinate. Table 1 summarizes the residual errors in geocoding the AIRSAR images. The geocoding accuracy indicated by table 1 was verified by Visual comparison between the geocoded images and an overlaid transparent copy of the topographic map (in scale 1:25 000).

In the resampling process, a Gaussian weighting function was used to resample each output pixel. In this type of resampling, the amount of speckle reduction is controlled by the width of the weighting function. In resampling of the August-89 scene, the standard deviation of the weighting function was 0.8 pixels in slant range and 0.8 pixels in azimuth. This means that the standard deviation was approximately 70 percent of the pixel spacing (12.5 m) of the geocoded images. In the June-91 and July-91 scenes, less speckle reduction was required due to lower speckle level in the 16-look images. The standard deviation of the weighting function was 0.35 pixels in slant range and 0.5 pixels in azimuth, approximately 25 percent of the pixel spacing of the geocoded images in range and 50 per cent in azimuth.

Table 1. Summary of geocoding accuracy

Scene	Number of GCPs	RMSE (pixels)		RMSE (m)	
		Range	Azimuth	Range	Azimuth
August-89	23	1.6	1.1	14.6	13.3
June-91	28	1.6	1.4	14.6	16.9
July-91	24	1.2	0.8	10.7	9.7

The geocoded Stokes matrix images were normalized for terrain topography:

$$P_{norm} = P_{orig}\frac{\tan(\theta_r)}{\tan(\theta_{nom})} \quad (1)$$

where P_{norm} is the normalized Stokes matrix element, P_{orig} the original Stokes matrix element, θ_r the incidence angle in range direction (depending on the local slope), and θ_{nom} the nominal incidence angle depending only on the range co-ordinate.

Stand-wise average Stokes matrices were computed using the digitized forest map. For stands greater than 100 pixels (approximately 1.7 ha) only those pixels were included in the averaging whose average power (the Stokes matrix element F_{11}) was at most 50 percent smaller and at most 70 percent larger than the stand-wise average power. This was done to eliminate the effects of inhomogeneous stand closure (shadows due to small openings and high return from the far edge of small openings) on the stand-wise average Stokes matrix.

After stand-wise averaging, the stands larger than a threshold (1 ha or 2 ha depending on the analysis) were selected to be used in further analyses.

2.4 Analysis Methods

As previously (Rauste 1992a), polarization synthesis was used to find the optimum polarization for forest biomass mapping. The whole space of all possible polarization combinations (combinations of transmit orientation, transmit ellipticity, receive orientation, and receive ellipticity) were traversed in a grid of 5 to 15 degrees. For each polarization combination:

- the received power was calculated for each stand based on the stand-wise Stokes matrix.
- the correlation coefficient between the received amplitude (square root of the received power) and the forest stem volume was calculated.

Changes in backscattering as a function of time were studied using three techniques:

- plotting the (relative) backscatter amplitudes of forest stands as a function of time,

- scatter plots of data from two dates, and
- visual interpretation of colour composites and principal components made of images of three dates.

In the first technique, the development of each stand was plotted as a line from the first image to the last. Because no absolute calibration was applied to the data, the datasets of different dates were normalized by forcing the average power (computed over all stands of the data set) to the same value.

3 RESULTS

3.1 Radar-Biomass correlation

Table 2 shows the correlation between radar amplitude and forest stem volume. Only stands larger than 1 ha were included in the table. For C and L bands, the correlations (table 3) were computed also for relatively young forests with the stem volume less or equal to 100 m^3/ha. The P-band HV-polarization has the highest correlation. The C and L-bands have also a relatively high correlation with stem volume, especially in forests where the stem volume is relatively small. The C and L-band correlations are higher than what was obtained earlier with the August 1989 data only (Rauste et al. 1992). The difference is explained by the fact that only stands larger than 1 ha were included in this study. Only the basic linear polarizations (HH, VV, and HV) are included in table 2. In the search for optimal polarization (section 2.4), the strongest correlations between the radar backscatter and stem volume were found in P-band and always close to the HV-polarization. The somewhat lower correlations in P-band of the June-91 scene may be due to deficiencies in antenna pattern correction.

Table 2. Correlation between radar amplitude and stem volume

Scene	Band	Stem Volume (m^3/ha)	Number of stands	HH	VV	HV
August-89	C	0 ... 830	179	-0.392	-0.078	-0.429
June-91	C	0 ... 830	183	-0.460	-0.199	-0.349
July-91	C	0 ... 830	181	-0.583	-0.260	-0.507
August-89	L	0 ... 830	182	-0.161	-0.046	-0.268
June-91	L	0 ... 830	184	-0.176	0.134	-0.123
July-91	L	0 ... 830	179	-0.262	0.082	-0.266
August-89	P	0 ... 830	182	0.280	0.210	0.750
June-91	P	0 ... 830	176	0.230	0.216	0.590
July-91	P	0 ... 830	179	0.272	0.234	0.707

Table 3. Correlation between radar amplitude and stem volume for young stands

Scene	Band	Stem Volume (m^3/ha)	Number of stands	HH	VV	HV
August-89	C	0 ... 100	36	0.315	0.575	0.215
June-91	C	0 ... 100	37	0.107	0.631	0.491
July-91	C	0 ... 100	36	-0.062	0.667	0.386
August-89	L	0 ... 100	37	0.539	0.674	0.671
June-91	L	0 ... 100	37	0.635	0.584	0.637
July-91	L	0 ... 100	35	0.684	0.679	0.699

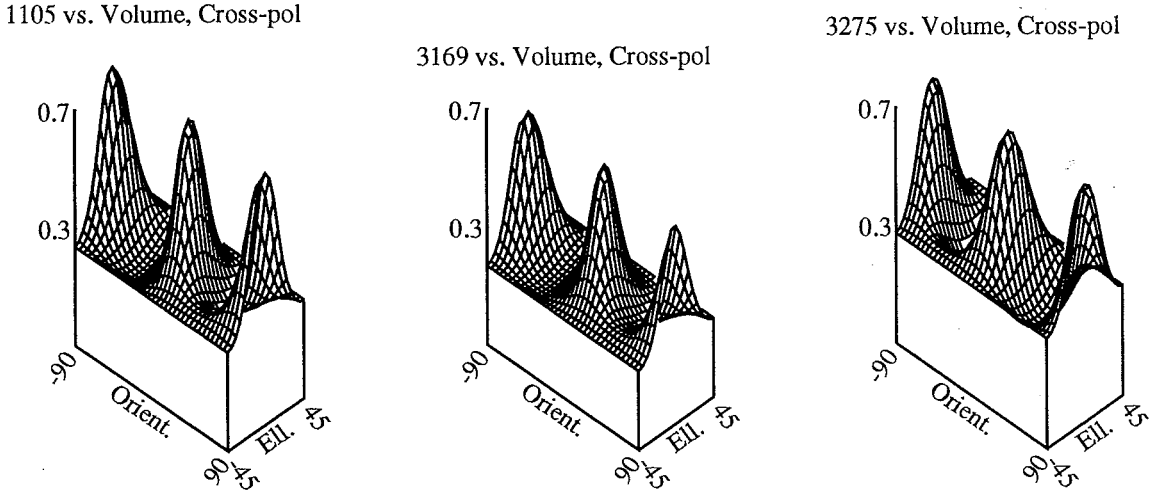

(a) August 1989 (b) June 1991 (c) July 1991

Figure 1. Radar-biomass correlation as a function of polarization (P-band, cross-polarization)

The P-band biomass correlation depends strongly on the polarization as observed in a previous study (Rauste 1992a). Figure 1 shows the correlation coefficient between cross-polarized P-band amplitude and stem volume as a function of polarization. The same pattern can be seen in all 3 diagrams. The highest correlations are found in the vicinity of the original HV polarization.

A linear multiple regression model was determined for the forest stem volume (as dependent variable) with the P-HV radar data of the three dates as the independent variables. Stand-wise average

Stokes matrix data of stands larger than 2 ha were used in the model. A multiple correlation coefficient of 0.82 (coefficient of determination 0.68) was obtained. The correlation was higher than the highest single-date correlation coefficient (August 1989: 0.79, June 1991: 0.60, and July 1991: 0.75) using the same data set. Figure 2 shows the residuals and 5-percent confidence limits of the model.

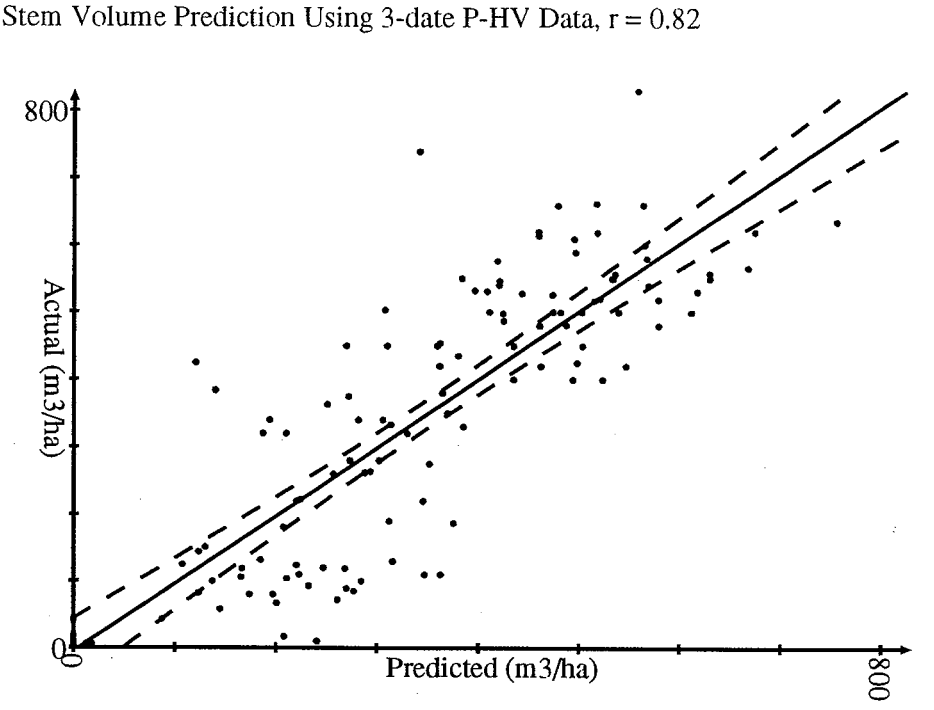

Figure 2. A tri-temporal regression model for forest stem volume

3.2 Backscattering as a function of time

Figure 3 shows the C, L, and P band amplitude as a function of time. In C-band, the June-91 values in HH are higher than the August-89 or July-91 values. In VV, the situation is the opposite. This is most likely due to the lacking channel imbalance calibration of the June-91 scene. Inspection of some corner reflector pixels in the June-91 scene showed that the HH amplitude is some 5 to 10 percent higher than the VV amplitude.

In general, the backscatter changes of forest stands are relatively small. Comparing the direction and magnitude of change with ground data does not reveal an obvious and easily identifiable reason for the change in average backscatter. Clear-cut areas form an exception to this observation. Inspection of the tri-temporal colour composites suggests that the correction of antenna pattern effects in the June-91 scene may have been slightly too cautious.

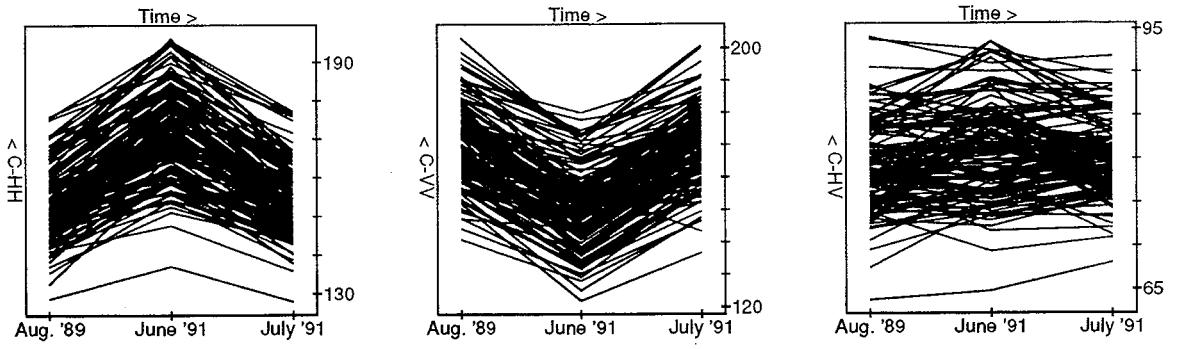

(a) C-HH. (b) C-VV. (c) C-HV.

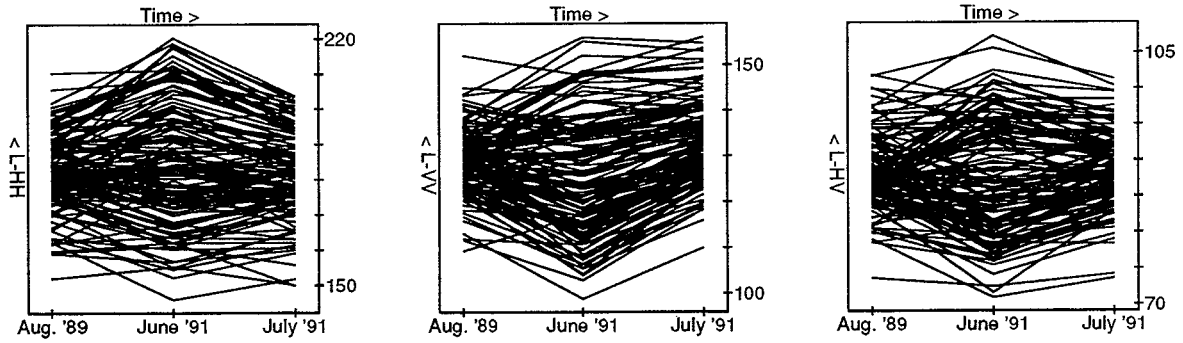

(d) L-HH. (e) L-VV. (f) L-HV.

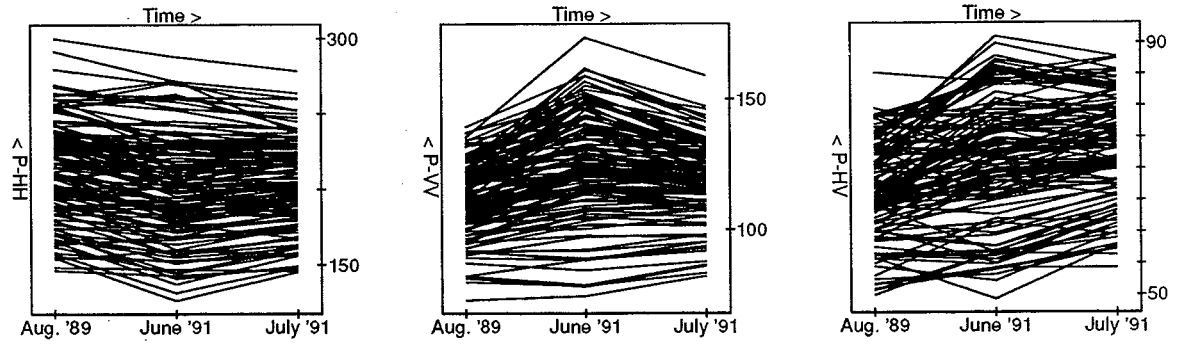

(g) P-HH. (h) P-VV. (i) P-HV.

Figure 3. Backscatter amplitude as a function of time

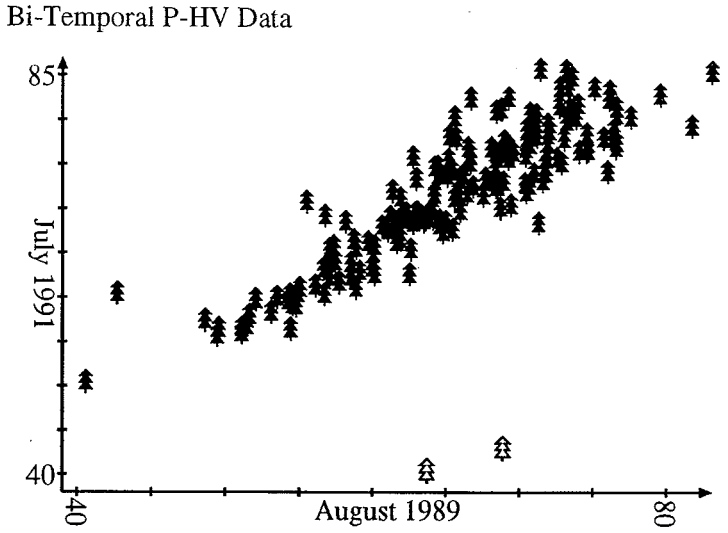

Figure 4. P-HV of July 1991 *vs.* P-HV of August 1989

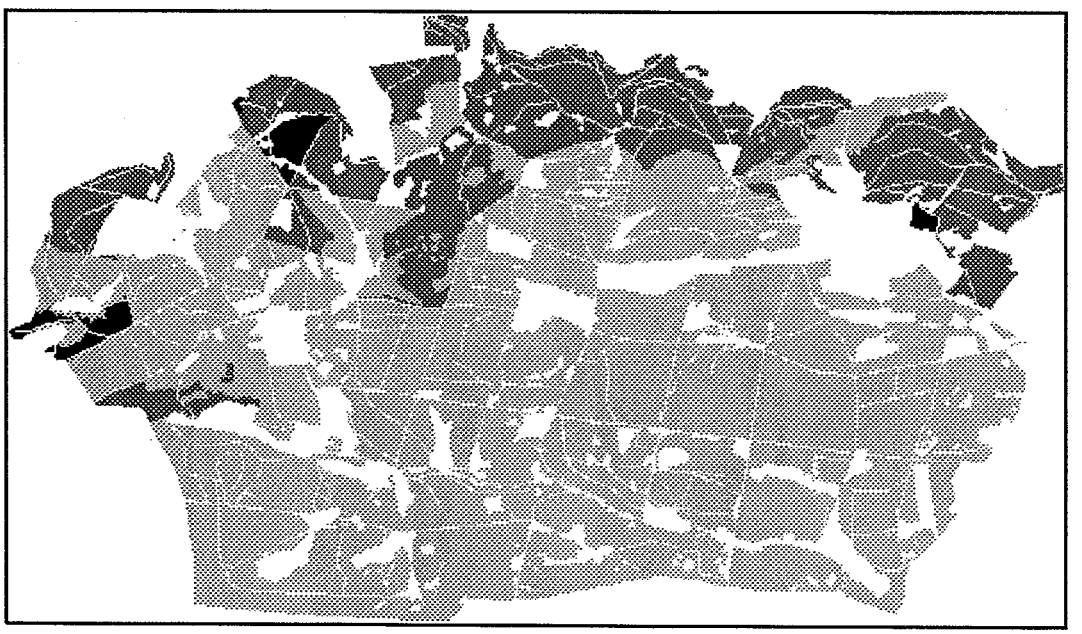

Figure 5. P-HV backscatter change by forest stands

Clear-cut areas can be identified clearly in tri-temporal colour composites in P-band, but also in L and C-bands. By visual evaluation, the contrast between the clear-cut areas and forests is largest in P-band, then in L-band and smallest in C-band. Figure 4 shows a scatter diagram of forested (solid symbols) and two clear-cut stands (outlined symbols). Figure 5 shows the direction of change of the P-HV backscatter in stands larger than 2 ha. Stands where P-HV backscatter of 1989 was higher than that of 1991 are shown in black. This area includes the clear-cut area near the eastern end of the picture. Stands where the P-HV backscatter of 1989 falls between the June and July values of 1991 are shown in dark gray. Stands where both the June and July values of 1991 are higher than that of 1989 are shown in light gray. The areas where the P-HV backscatter has decreased most are concentrated in the northern part of the study site. The reason for this could be more intensive thinning cutting in these areas. This was not verified because no quantitative information on recent thinning cutting were available in this study.

4 DISCUSSION

The high correlations between the mixed-forest biomass and P-HV backscatter obtained earlier (e.g. Rauste 1992a) were verified in this study. Also the strong dependence of the correlation on the polarization was verified. A spaceborne P-band SAR using HV-polarization could be a useful tool in mapping large forested areas in the boreal forest zone.

The results on the development of backscatter with time of the year should be considered preliminary. Further research with more thoroughly calibrated data is needed to obtain information on the development of the backscatter characteristics of different types of forest with different amounts of biomass.

The separability of clear-cut areas could be studied using the same kind of optimal polarization search as used in the correlation analysis. If data on the thinning cutting were available, the potential to map small changes could be studied using the same type of techniques.

5 REFERENCES

Christensen, N., Kasischke, E. and Dobson, M. 1990. SAR-derived estimates of aboveground biomass in forested landscapes, Proceedings of the International Geoscience and Remote Sensing Symposium *IGARSS'90,* University of Maryland, College Park, Maryland, USA, May 20-24, 1990, p. 1209-1212.

Churchill, P. and Attema, E. 1991. The European airborne polarimetric SAR campaign MAESTRO 1, Proceedings of the International Geoscience and Remote Sensing Symposium *IGARSS'91,* Helsinki University of Technology, Espoo, Finland, June 3-6, 1991, Vol. II, p. 327-328.

Held, D., Brown, W., Freeman, A., Klein, J., Zebker, H., Sato, T., Miller, T., Nguyen, Q., and Lou, Y. 1988. The NASA/JPL multifrequency, multipolarization airborne SAR system, Proceedings of the International Geoscience and Remote Sensing Symposium *IGARSS'88,* Edinburgh, September 1988, p. 345-350.

Dubois, P. & Norikane, L. 1987. Data volume reduction for imaging polarimetry, Proceedings of *IGARSS'87* Symposium, Ann Arbor, 18-21 May 1987, p. 691-696.

Hussin, Y., Reich, R., and Hoffer, R. 1991. Estimating slash pine biomass using radar backscatter, *IEEE Transactions on Geoscience and Remote Sensing,* Vol. 29, No. 3, May 1991, p. 427-431.

Kasischke, E., Bourgeau-Chavez, L., Christensen, N., and Dobson, C. 1991. The relationship between aboveground biomass and radar backscatter as observed on airborne SAR imagery, Proceedings of the Third Airborne Synthetic Aperture Radar (AIRSAR) Workshop, May 23-24 1991, *JPL-Publication* 91-30, p. 11-21.

Rauste, Y. 1991. Polarimetric radar signatures of forest as a function of terrain topography. Proceedings of the International Geoscience and Remote Sensing Symposium *IGARSS'91,* Helsinki University of Technology, Espoo, Finland, June 3-6, 1991, Vol. II, p. 341-344.

Rauste, Y. 1992a. Estimation of biomass in mixed forests using polarimetric SAR data, Proceedings of *IGARSS'92,* South Shore Harbour Resort and Conference Center, Houston, Texas, May 26-29, 1992, p. 789-791.

Rauste Y. 1992a. Geometric/radiometric preprocessing of SAR scattering matrix data, Proceedings of the Final Workshop of the MAESTRO/AGRISCATT Campaigns, Noordwijk, 6-7 February 1992, p. 113-116.

Rauste, Y., Heiska, K., and Pulliainen, J. 1992. On forest inventory and elevation determination using polarimetric radar data, Proceedings of the Final Workshop of the MAESTRO/AGRISCATT Campaigns, Noordwijk, 6-7 February 1992, p. 117-121.

Rignot, E., Way, J., Mc Donald, K., Viereck, L., and Adams, P. 1992. Monitoring of environmental conditions in the Alaskan forests using ERS-1 SAR data, Proceedings of *IGARSS'92,* South Shore Harbour Resort and Conference Center, Houston, Texas, May 26-29, 1992, p. 530-532.

Sader, S. 1987. Forest biomass, canopy structure, and species composition relationships with multipolarization L-band synthetic aperture radar data, *Photogrammetric Engineering and Remote Sensing,* Vol. 53, No. 2, February 1987, p. 193-202.

Le Toan, T. and Beaudoin, A. 1991. Relating forest parameters to SAR data, Proceedings of the International Geoscience and Remote Sensing Symposium *IGARSS'91,* Helsinki University of Technology, Espoo, Finland, June 3-6, 1991, Vol. II, p. 689-692.

Zebker, H. and Lou, Y. 1990. Phase calibration of imaging radar polarimeter Stokes matrices, *IEEE Transactions on Geoscience and Remote Sensing,* Vol. 28, No. 2, p. 246-252.

van Zyl, J. 1990. Calibration of polarimetric radar images using only image parameters and trihedral corner reflector responses, *IEEE Transactions on Geoscience and Remote Sensing,* Vol. 28, No. 4, p. 337-348.